

Force and Velocity Measured for Single Kinesin Molecules

Karel Svoboda*† and Steven M. Block*‡

*Rowland Institute for Science

100 Edwin Land Boulevard

Cambridge, Massachusetts 02142

†Graduate Committee on Biophysics

Harvard University

Cambridge, Massachusetts 02138

‡Department of Molecular Biology

Princeton University

Princeton, New Jersey 08544

Summary

We measured the force-velocity curves of single kinesin molecules attached to silica beads moving in an in vitro motility assay. Optical trapping interferometry was used to track movement with subnanometer precision and to apply calibrated, pN-sized forces to the beads. Velocity decreased linearly with increasing force, and kinesin molecules moved against applied loads of up to 5–6 pN. Comparison of force-velocity curves at limiting and saturating ATP concentrations suggests that the load-dependent diminution in kinesin velocity may be due to a decrease in the net displacement per molecule of ATP hydrolyzed, not simply to a slowing of the ATP turnover rate; kinesin would therefore appear to be a loosely coupled motor.

Introduction

Motor proteins, or mechanoenzymes, are molecules that convert chemical energy into mechanical work. Measurements of force and velocity have long formed the basis for quantitative modeling of these macromolecules, but movement in traditional contractile systems is generated by large numbers of interacting components. In muscle fibers, millions of myosin molecules function during contraction, while bending in eukaryotic flagella is produced by thousands of dynein molecules. Such enormous numbers complicate interpretation in terms of molecular mechanochemistry. In recent years, in vitro motility assays have facilitated increasingly quantitative studies using limited numbers of molecular motors under relatively well-defined conditions, free of the complex regulatory elements typically present in vivo. Single molecules of the molecular motor kinesin can move loads over distances of several micrometers, corresponding to hundreds of mechanochemical events (Howard et al., 1989; Block et al., 1990), making this system very attractive for the study of molecular mechanochemistry.

Kinesin has a very low basal ATPase rate (Vale et al., 1985), with a fast phosphate release and a rate-limiting ADP release (Hackney et al., 1989). ADP release can be accelerated up to 1000-fold by microtubules (MTs), and the MT-activated ATPase obeys Michaelis–Menten kinetics

(Kuznetsov and Gelfand, 1986; Hackney, 1988). The overall reaction scheme is similar to that of myosin (equation 1):



Since kinesin molecules rarely release MTs, K stands for the kinesin–MT complex. In contrast with myosin, $k_3 \gg k_{-2}$; i.e., essentially no hydrolysis reversals occur per product released (Hackney, 1988). Although a number of studies of MT-activated kinesin ATPase have been performed, there is little consensus as to the maximum value of the turnover rate per kinesin molecule, k_{cat} , particularly under conditions that obtain for in vitro assays (Kuznetsov and Gelfand, 1986; Cohn et al., 1987; Hackney, 1988; Hackney et al., 1991; Gilbert and Johnson, 1993). Part of the problem may be traceable to differences in protein source, purification methods, assay buffers and conditions, etc., but erratic variations in turnover rate among preparations under nominally identical conditions have also been noted (Hackney et al., 1989). Typical values for k_{cat} (3/s for the native heterotetrameric form [Hackney et al., 1991]) would seem to be incompatible with single-molecule speeds of ~500 nm/s and a molecular step size of 8 nm (Svoboda et al., 1993), assuming a mechanism where one ATP is hydrolyzed per step (1:1 coupling). It has therefore been suggested that mechanoenzymes might somehow undergo several steps per ATP hydrolyzed (1:many coupling) (Yanagida et al., 1993; Taylor, 1993), an explanation first advanced to explain discrepancies in measurements in the actomyosin system (Yanagida et al., 1985; Burton, 1992). An alternative explanation may be that the turnover rate achieved by kinesin in vitro is substantially higher than the average value measured in solution. In support of this explanation, Hackney has recently found that native kinesin molecules in solution are mostly in a closed conformation, with the tail folded back against the motor domain (Hackney et al., 1992). Recombinant fragments of kinesin molecules, consisting of dimers of motor domains without the tail, have substantially higher turnover rates ($k_{cat} \approx 90/s$), consistent with 1:1 coupling (Hackney, 1994). Together, these observations suggest that a majority of kinesin molecules in solution might exist in an inactive form, with the overall turnover arising from a minority fraction of activated molecules.

ATP-dependent velocities of single kinesin molecules in vitro follow the Michaelis–Menten relationship,

$$v(c) = \frac{v_{max}c}{K_m + c}$$

(equation 2), where c is the ATP concentration, v_{max} is the velocity at saturating ATP, and K_m is a mechanochemical Michaelis–Menten constant (Howard et al., 1989). Kinesin moves parallel to the MT protofilament (Ray et al., 1993; Kamimura and Mandelkow, 1992; Gelles et al., 1988). Ad-

vances in optical trapping (Svoboda and Block, 1994) and subnanometer-level tracking (Denk and Webb, 1990) have provided evidence for molecular steps during the transport of silica beads by kinesin molecules along MTs: individual kinesin molecules advance in discrete increments of 8 nm (Svoboda et al., 1993). At limiting concentrations of ATP ($c \ll K_m \approx 90 \mu\text{M}$ for these experiments), steps appear at random without clustering, suggesting that each ATP hydrolysis is responsible for at most one step (Svoboda et al., 1993).

To understand the mechanism of force production, it is necessary to go beyond kinematic measurements and to probe the load-dependent chemistry of motor proteins. Recent estimates of the maximum force produced by kinesin molecules have generated disparate results: 1.9 ± 0.4 pN measured with optical tweezers in a MT gliding assay (Kuo and Sheetz, 1993), ≥ 5 pN measured with optical tweezers in a moving-bead assay (Svoboda et al., 1993), and 0.12 ± 0.03 pN measured with a centrifugal microscope in a sperm gliding assay (Hall et al., 1993). Here, we used optical trapping interferometry to measure force-velocity curves for single kinesin molecules at two different ATP concentrations. We found that the stall force for kinesin molecules is 5–6 pN, higher than some estimates, but consistent with our earlier work (Svoboda et al., 1993). A comparison of force-velocity curves at different ATP concentrations suggests that the slower movement of kinesin molecules under increasing load may be due to a load-dependent decrease in the net distance traveled per ATP hydrolyzed.

Results

In a typical experiment, a silica bead coated with a small number of kinesin molecules (fewer than one molecule per bead, on average) was captured out of a suspension and deposited onto a MT using optical tweezers. A single kinesin molecule subsequently attached to the MT and began movement, developing load as it pulled the bead toward the edge of the optical trap. After a bead was deposited, the trap was held stationary, and bead position was tracked with subnanometer accuracy using interferometry. For displacements of up to ~ 200 nm, the force is proportional to displacement from the trap center, and this constant of proportionality can be measured. The trap therefore acts as a calibrated Hookeian spring on the kinesin molecule, acting through the bead. Motors moved a few hundred nanometers before releasing from the MT, whereupon the bead would return to the trap center, reattach, and begin movement anew. In this fashion, an individual kinesin molecule could be studied for up to several minutes and up to hundreds of mechanochemical events, until, for whatever reason, the motor failed to bind to the MT or became stuck irreversibly (Svoboda et al., 1993).

Optical Trapping Interferometry

The optical trapping interferometer (Svoboda et al., 1993) consists of optical tweezers (a single-beam gradient force optical trap) (Ashkin et al., 1986) combined with a dual-beam interferometer (Denk and Webb, 1990) (Figure 1).

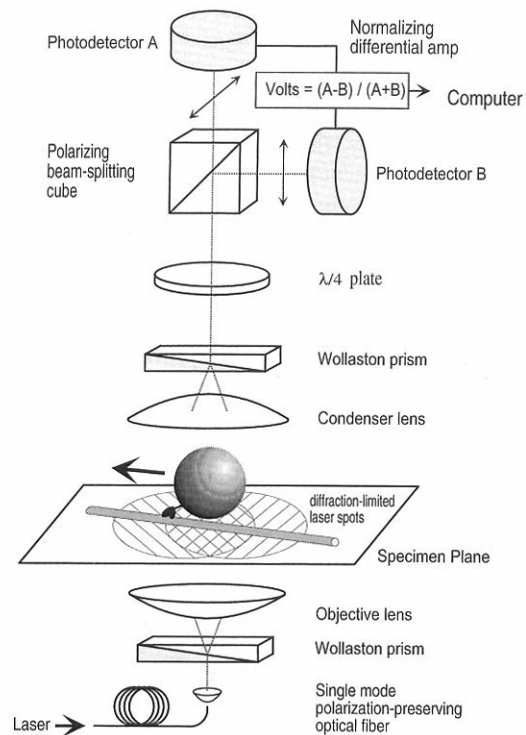


Figure 1. Schematic of the Optical Trapping Interferometer and the Motility Assay

For description, see text.

Polarized laser light is introduced into a microscope equipped with differential interference contrast (DIC) optics at a point just below the objective Wollaston prism. The prism splits this light into two beams with orthogonal polarizations that are focused to two overlapping, diffraction-limited spots in the specimen plane. Together they act as a single optical trap. A transparent object located in the region illuminated by the spots (the detector zone) introduces a relative phase retardation between them. When the beams are recombined in the Wollaston prism at the condenser back focal plane, elliptically polarized light is produced. The degree of ellipticity is measured using additional optics and provides a sensitive measure of displacement, passing through zero when the object is located symmetrically between the two spots. The interferometer is essentially a one-dimensional position detector: its signal is most sensitive along the Wollaston shear direction and relatively insensitive to movements in other directions (Denk and Webb, 1990). During measurement, assays were monitored simultaneously by video-enhanced DIC microscopy, which can visualize single MTs (Schnapp, 1986).

The response of the interferometer was calibrated in a series of steps. We first calibrated the x - y piezo stage, which held a test specimen consisting of highly uniform silica beads affixed to the coverglass of a flow chamber. As a bead was driven past the detector, its position with respect to the center of the trap was compared with the interferometer output voltage, V_{out} , to construct a response

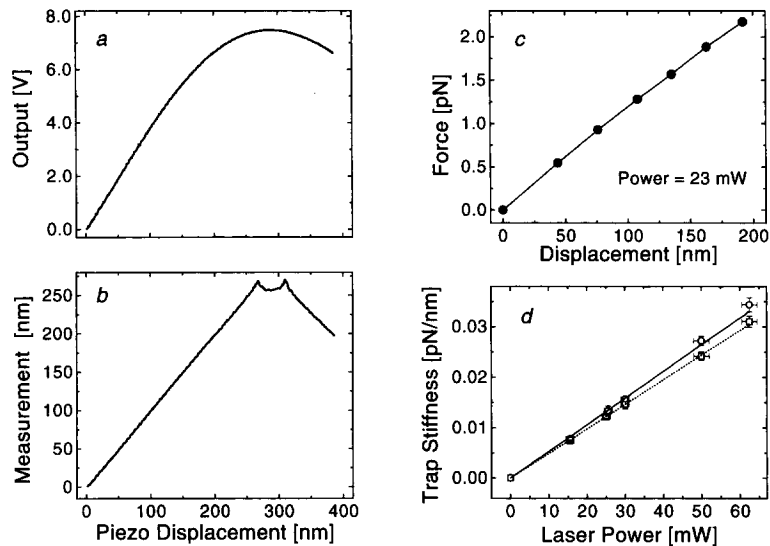


Figure 2. Calibration of the Optical Trapping Interferometer

(a) Response curve of the interferometer. An immobilized silica bead was driven at constant velocity ($0.91 \mu\text{m}$) through the interferometer detector zone by the piezo stage. Interferometer output is plotted as a function of displacement from the center of the trap.

(b) Measured displacement as a function of piezo displacement after calibration.

(c) Trap stiffness measurement. A free bead was trapped $2 \mu\text{m}$ above the coverglass surface and a viscous force was applied, as described in the text. The slope of the force as a function of bead displacement curve gives the stiffness.

(d) Trapping stiffness as a function of laser power at the specimen plane in water (circles) and assay buffer (squares). Stiffnesses were determined from the rolloff frequency of the power spectrum of Brownian fluctuations.

curve for the system (Figure 2a). A cubic polynomial was then fitted to this nonlinear response curve, and the fit parameters were subsequently used to determine displacement out to 200 nm directly from V_{out} (Figure 2b). Further calibration measurements with immobilized beads showed that displacement measurements over this range were accurate to $\pm 5\%$. Instrumentation noise was below $0.1 \text{ nm}/\sqrt{\text{Hz}}$ (Svoboda et al., 1993).

To calibrate optical forces, trapped silica beads were displaced with a viscous force by moving the piezo stage sinusoidally while bead displacement was measured by interferometry. Displacement from the trap center was linear with force over the range 0–200 nm (Figure 2c); the force profile of the optical trap could therefore be characterized over this range by the trap stiffness, α_r . During experiments, the trap stiffness for individual beads was measured by computing the power spectrum for Brownian fluctuations in position; this spectrum is Lorentzian, with a corner frequency, f_c , related to the stiffness through $f_c = \alpha_r/2\pi\beta$. The viscous drag coefficient of a bead was computed as $\beta = 6\pi\mu\xi a$, where a is the particle radius, μ is the viscosity of the surrounding medium, and ξ is a correction factor for the proximity of the surface (in this work, $\xi = 1.08$, $2 \mu\text{m}$ from the surface) (Svoboda and Block, 1994). Trap stiffness was proportional to laser power at the specimen plane, P (Figure 2d), and trap forces were essentially independent of the distance from the surface over 0–2 μm .

Bead Assay

Silica beads were first coated with casein and then incubated with low concentrations of kinesin. We used flow chambers in which the lower coverglass was pretreated with 4-ABDMS (4-aminobutyltrimethoxysilane) to produce a surface that binds MTs. MTs were introduced into the chamber at relatively high flow rates, which ensured that they bound with their long axis parallel to the flow field. The chamber was mounted with its flow field

parallel to the Wollaston shear direction, so MTs became aligned with the interferometer. To our surprise, we found that this procedure yielded $>75\%$ of MTs bound with their plus ends pointing upstream. The reason for this asymmetry remains unknown, but it implies a preferential affinity of the plus end for this surface. Kinesin-coated beads were then introduced into the flow chamber.

A diffusing bead was captured with optical tweezers and held against a MT for a few seconds. When a bead did not move, we briefly shuttered the laser beam and repositioned the bead against the MT. This was repeated for three trials; the probability that a bead would move after further trials was negligible. At low laser powers, we distinguished two outcomes: first, the bead bound and moved, with probability $P(f)$, where f is the relative kinesin concentration, or second, the bead failed to bind, with probability $1 - P(f)$; under these conditions, beads rarely bound without moving ($\sim 1\%$). If single kinesin molecules move beads, then $P(f) = 1 - \exp(-\lambda f)$ corresponds to the Poisson probability that a bead carries one or more motors, where λ is a fitting parameter. Similarly, $1 - P(f) = \exp(-\lambda f)$ is the probability that a bead carries no motors. This form of $P(f)$ fits our data well (reduced $\chi^2 = 1.1$ [Bevington, 1969]) (Figure 3). Alternatively, if two or more motors were required to move a bead, one would expect $P(f) = 1 - \exp(-\lambda f) - (\lambda f)\exp(-\lambda f)$; this form did not fit our data well (reduced $\chi^2 = 2.1$; data not shown). We conclude that single kinesin molecules suffice to move beads, confirming earlier work (Howard et al., 1989; Block et al., 1990). Force-velocity experiments were performed at dilutions such that $P(f) \leq 0.5$, so that the probability that a bead carried two or more motors was <0.14 . Assuming a random distribution of motors over the bead surface, and allowing an 80 nm reach for the kinesin tether (Hirokawa et al., 1989; Scholey et al., 1989), we estimate the probability of two randomly attached kinesin molecules simultaneously binding a MT to be <0.02 .

At high laser powers, the fraction of moving beads was

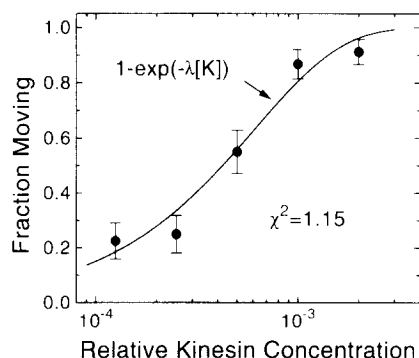


Figure 3. The Fraction of Beads Moving, p_m , as a Function of Relative Kinesin Concentration

The fit curve is given by $1 - \exp(-\lambda f)$, the Poisson probability that one or more kinesin molecules are bound to a bead. Values are expressed as $p_m \pm (\rho_m(1 - p_m)/N)^{1/2}$ and are the result of 40 measurements.

slightly lower, with optical damage likely to be a factor. One measure of optical damage was estimated by holding kinesin-coated beads in the trap for varying lengths of time before depositing them onto MTs. We then compared the fraction of beads not moving, including those exhibiting anomalously slow movement, intermittent movement, or both, for various periods of irradiation. The estimated half-life times power for movement in the trap was ~ 35 min \cdot mW. Even at the highest power used (62.5 mW), therefore, hundreds of mechanochemical events of an individual kinesin molecule could be observed.

Measurement of Kinesin Velocity

Bead-MT linkages display considerable flexibility (Svoboda et al., 1993). As beads move toward the edge of the optical trap and load increases, these linkages become increasingly stretched, and the bead velocity falls below the kinesin motor velocity. To derive the motor velocity from the measured bead velocity, it was necessary to characterize the elasticity of the linkage. Kinesin-coated beads were bound to MTs in the presence of the nonhydrolyzable ATP analog AMP-PNP, which produces a rigorlike association between the kinesin molecule and the MT. The piezo stage was then moved at a constant speed, v_s , while the bead velocity, v_b , was measured as a function of position. The ratio of these speeds is identical to the ratio of distances moved by the stage and the bead, and is given by $v_b/v_s = \alpha_{mot}/(\alpha_{mot} + \alpha_{tr})$, where α_{mot} is the strain-dependent elasticity of the bead-MT linkage. For all power levels, v_b/v_s increased rapidly up to bead displacements ~ 50 nm from the trap center. Beyond this distance, v_b/v_s was roughly constant out to the edge of the trap (Figure 4). The scatter in the data comes from the Brownian motion of tethered beads as well as from linkage heterogeneity. Measured bead velocities were divided by the experimentally determined value of $\langle v_b/v_s \rangle$ (averaged over the range 50–200 nm) to derive motor velocities. $\langle v_b/v_s \rangle$ at 15 mW is in close agreement with the elastic correction applied to our earlier step size measurements at moderate ATP concentrations and low load (cf. Figure 4 of Svoboda et

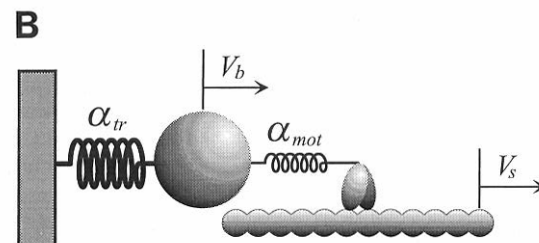
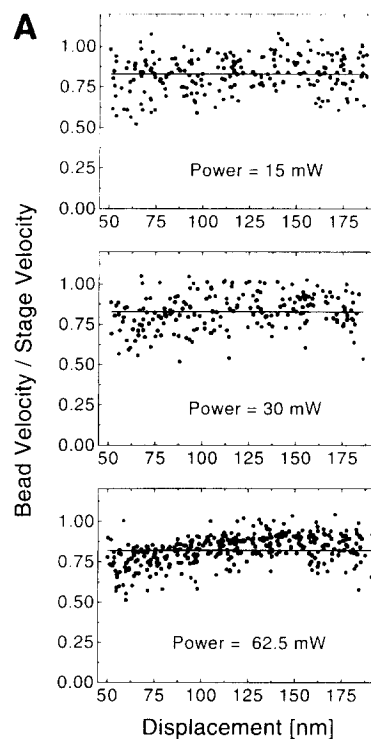


Figure 4. Elasticity of the Bead-MT Linkage

The ratio of bead velocity to stage velocity is shown as a function of bead displacement from the trap center. Ratios averaged over 50–200 nm were 0.83 ± 0.08 (62.5 mW), 0.84 ± 0.11 (30 mW), and 0.84 ± 0.11 (15 mW) and were roughly constant. Although the ratio v_b/v_s was approximated by a constant in converting bead velocity to kinesin velocity, this quantity actually increases monotonically with displacement for all power levels. This rise is quantitatively consistent with the requirement that the passive compliance α_{mot} be a monotonically increasing function of load, independent of the trap stiffness α_{tr} .

al. [1993]). The stress-strain curves for kinesin molecules bound to MTs in the absence of nucleotides (in true rigor) were similar. At the highest trap stiffnesses used, the total stretch in the bead-MT linkage was 204 ± 11 nm (mean \pm SEM, $n = 11$), which implies a relatively long tether length, $l = 65$ nm (Figure 5).

Applying very high loads to beads bound to MTs via kinesin in a rigorlike state showed that the bond is exceedingly strong; it supports forces in excess of 10 pN. A reliable estimate could not be determined in this work, however. First, at high tensions, MTs were sometimes pulled off the coverglass surface, rather than beads off the MT. Second, beads would occasionally dissociate at ~ 10 pN, but later withstood much higher loads after rebinding, or

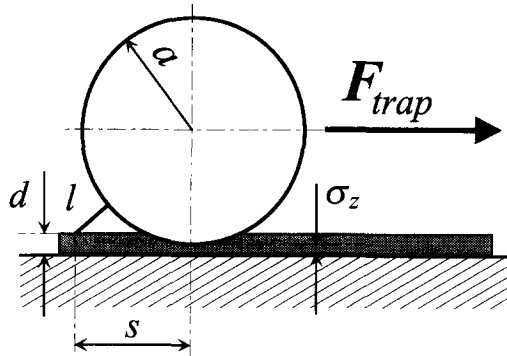


Figure 5. Geometry of the Bead Assay

The kinesin tether (bead–MT linkage) has length l , connecting a bead of radius a to the surface via a microtubule with diameter d . The force of the trap produces a tension in the tether. This tension has a component normal to the surface and tends to pull the bead toward the surface. The thermal RMS distance of the bead over the surface is $\sigma_z = \sqrt{\langle z^2 \rangle} = (s/a)(kT/\alpha_s)^{1/2}$. We have neglected the vertical trapping stiffness in deriving this estimate. The tether must point toward the center of the bead, on average; otherwise, the tether would produce an unopposed torque on the bead. The maximal extension of the bead–MT linkage is $s = ((l + a)^2 - (a - d)^2)^{1/2}$, neglecting $\sqrt{\langle z^2 \rangle}$, and any possible stretching in the microtubule or the kinesin molecule. Note that in this picture, the elasticity of the bead–MT linkage is entirely entropic.

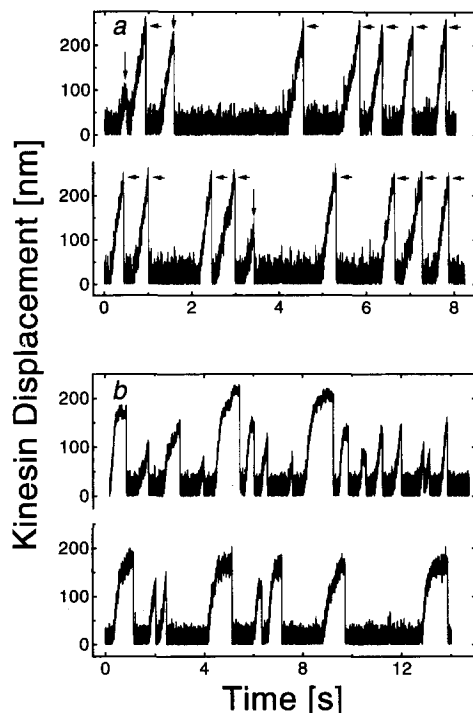


Figure 6. Examples of Multiple Runs at Saturating ATP Powered by Individual Motors

To derive the kinesin velocity, the bead velocity was corrected for the linkage flexibility (see text).

(a) Two examples at low load (15 mW). During most runs, beads escaped the trap without dissociating (horizontal arrows), but sometimes premature dissociations occurred (vertical arrows).

(b) Two examples at high load (62.5 mW). Beads almost never reached the edge of the trap and often dissociated before slowing down substantially. The algorithm to compute displacement returns the absolute value, so that distance from the center of the trap is rectified.

vice versa. Third, the tension sustained by the kinesin tether might be somewhat larger than the actual force applied to the bead, owing to the geometry of the linkage: the magnitude of this tension is $F_{trap}/\cos \theta$, where θ is the angle between kinesin tether and the coverglass surface, and F_{trap} is the force applied to the bead.

Load-Dependent Velocity

From earlier studies, it was apparent that kinesin motors could move against loads up to 5 pN, but not much higher (Svoboda et al., 1993). To study the load-dependent velocity, we measured speeds at three different laser power levels at each of two ATP concentrations. Light levels, and corresponding trapping stiffnesses, were chosen to cover the entire range of forces: 15 mW (0.40–1.58 pN), 30 mW (0.80–3.17 pN), and 62.5 mW (1.67–6.67 pN). One ATP concentration (10 μ M) was picked to be well below the apparent K_m for kinesin movement ($\sim 90 \mu$ M for these experiments), the other well above it (2 mM). At 15 mW and 30 mW, runs terminated in one of two ways: either a motor would drag the bead out of the trap altogether, or the motor would release from the MT substrate before reaching the edge of the trap. In either case, the bead was often recaptured by the trap and resumed movement (Figure 6a). At low power levels, up to 20 runs of ≥ 200 nm could be measured in this way using a single bead. At the highest power level (62.5 mW), few beads escaped the trap ($< 1\%$; Figure 6b). As beads moved out of the trap and developed load, motors slowed, sometimes to below 1% of the unloaded velocity (Figures 7 and 8). Such beads would generally resume movement at the unloaded velocity if the trapping light was shuttered ($n = 25$). The run length, defined as the distance traveled by a bead before release and return to the center of the trap, was significantly shorter at high loads (~ 100 nm at 62.5 mW) than at low loads (> 1000 nm at 15 mW; see Figure 6). At high loads, single steps could often be made out in displacement records, with a step size on the order of 8 nm, but noise and stage drift prevented our resolving all events. Apart from Brownian motion, displacement usually increased monotonically until bead release. Occasionally, the kinesin motor would appear to slip backward, and this happened more frequently at high loads than at low loads. Slipping was most apparent when the motor would alternate several times between positions 8 nm apart (Figure 8c).

Force-Velocity Curves

For each run, velocities were estimated by fitting lines to successive 20 nm segments of movement and plotted against the average force for each segment, resulting in a force–velocity curve. For each ATP concentration, force–velocity curves computed for individual runs at all power levels were averaged (Figure 9). This analysis procedure was tested using simulated data generated by computer, based on stochastic steppers subject to Gaussian noise. Simulations showed that velocity determinations from many runs (≥ 10) must be used to construct force–velocity curves, owing to the (presumably) stochastic nature of the stepping process and the limited number of steps per run (~ 20). At saturating ATP, kinesin velocity appeared to be

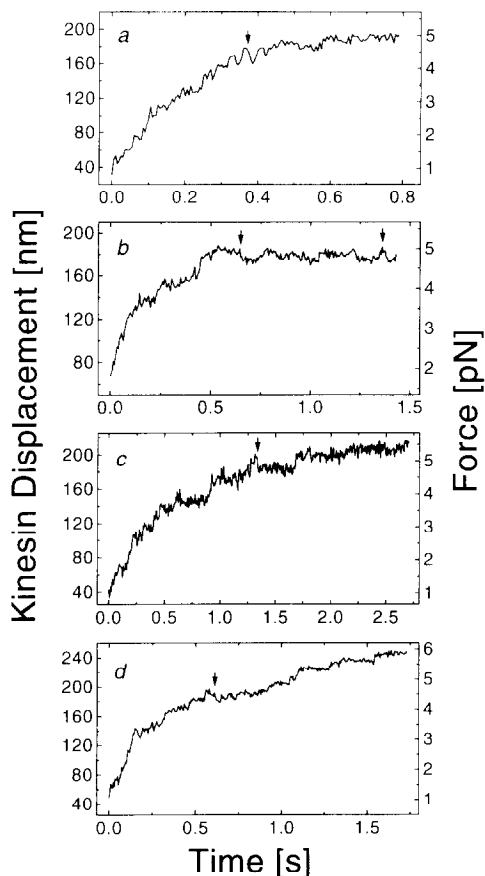


Figure 7. Examples of Multiple Runs at High Load (62.5 mW) and Saturating ATP (2 mM), Showing the Load-Dependent Diminution in Kinesin Speeds

Some examples of kinesin slippage are indicated by the arrows.

roughly independent of load out to ~ 1.5 pN (Figure 9a), although the scatter in the data prevents a clear resolution of this point. For increasing loads, velocity decreased almost linearly until stall. A linear fit of data from 1.5 to 5.0 pN gave an extrapolated maximal force (stall force) of 5.7 ± 0.4 pN. At limiting ATP, the data were somewhat noisier, and a plateau at lower loads was not observed. The extrapolated stall force, derived from a linear fit, was similar, 5.1 ± 0.5 pN (Figure 9b).

Forces were measured for three independent preparations of kinesin protein. In two cases, stall forces were identical to the pooled estimate above, even though one preparation was fresh, while the other had been stored at -20°C for nearly a year. A third fresh preparation gave a reproducibly smaller stall force (~ 4 pN at 2 mM ATP), even though the purification was nominally identical, suggesting that an unidentified modification of kinesin might alter its mechanochemistry without destroying motility altogether. Although data from the latter preparation were not used to compute kinesin forces, this raises the possibility that the shape of averaged force-velocity curves might reflect a polydispersity in stall forces among motors more than the mechanochemical properties of an individual protein. However, in several cases, records were sufficiently

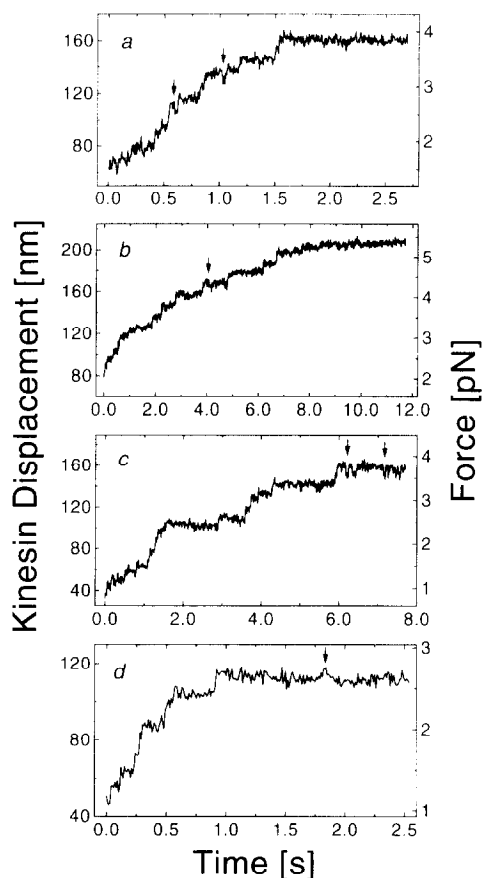


Figure 8. Selected Runs at High Load (62.5 mW) and Limiting ATP (10 μM), Showing the Load-Dependent Diminution in Kinesin Speed. Some examples of kinesin slippage are indicated by the arrows.

good to determine force-velocity curves for individual motor molecules (Figure 9c). Although such curves were noisy, they were generally consistent with our averaged force-velocity curves.

Discussion

The crossbridge model proposed by A. F. Huxley was among the first to explain existing data and made quantitative predictions for muscle (Huxley, 1957). In this model, thermally fluctuating myosin crossbridges associate with an actin filament in a strain-dependent manner, binding when at positive strain. Once bound, crossbridges exert force. The energy of ATP hydrolysis, binding, or both is used to break detailed balance in some unspecified manner, such that dissociation rates are small for positively strained crossbridges and large for negatively strained ones. The significance of this early model is that it demonstrated how a microscopic scheme for protein interaction could lead to sliding motion and thereby to muscle contraction. But since molecular details (in this case, the strain-dependent rates) are completely unknown, the model has many free parameters (strictly speaking, an infinite number), and the same can be said for other microscopic mod-

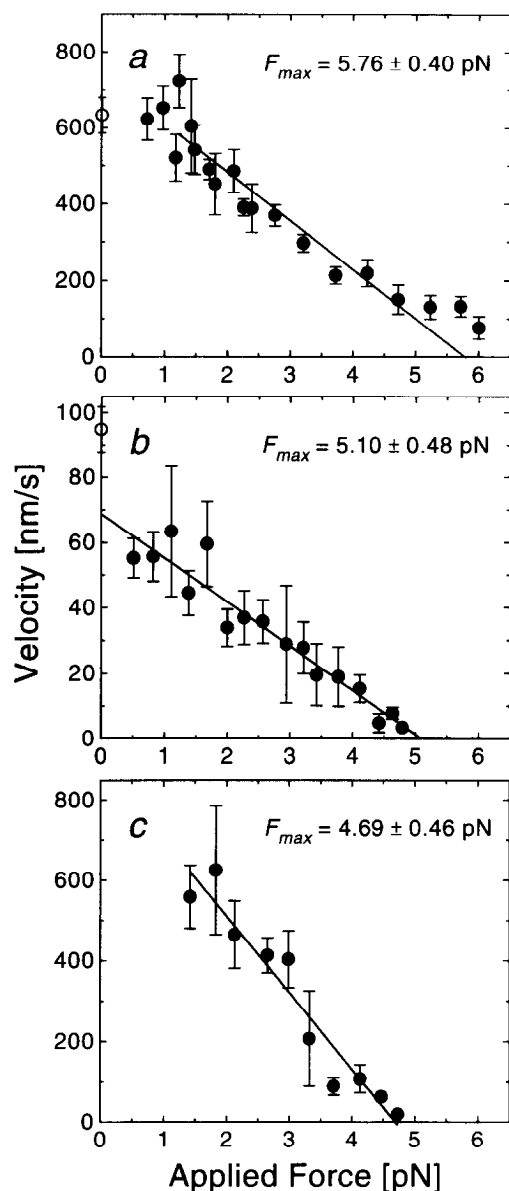


Figure 9. Force–Velocity Curves

Data from experiments at 15 mW, 30 mW, and 62.5 mW were pooled and binned (solid circles). Velocities at very low loads were measured using video tracking (open circles). Points represent mean velocity \pm SEM.

(a) Averaged force–velocity curve at 2 mM ATP. The solid line represents a fit to data in the range 1.5–5.0 pN. The velocity below 1.5 pN was roughly independent of load. Data points for >5 pN were not included in the line fit, because they came from a small number of measurements and contain data from two runs in which the beads were pulled entirely out of the trap; these events may have been caused by multiple kinesin motors.

(b) Averaged force–velocity curve at 10 μ M ATP.

(c) Force–velocity curve for individual kinesin motor at 2 mM ATP; only data at 62.5 mW could be measured.

els. Given the lack of dynamic, atomic-level information, we choose to take a phenomenological approach to modeling, independent of microscopic details of the system.

What is the effect of load on kinesin mechanochemistry? We define the coupling constant, ϵ , through $v = \epsilon \cdot d \cdot k_{cat}$,

where v is the average kinesin velocity and d is the step size; ϵ is therefore a measure of the number of steps made per ATP hydrolyzed. Does ϵ depend upon load? If ϵ were independent of load, then kinesin would be a tightly coupled machine, i.e., it would move with a fixed stoichiometry of displacement to hydrolysis, and the ATPase rate would decrease in proportion to velocity with increasing load. However, if ϵ were to change with load, kinesin would be a loosely coupled machine (Oosawa and Hayashi, 1986). We construct below a simple phenomenological theory of single-motor force–velocity curves and use it to distinguish between these scenarios.

Analysis of Force–Velocity Curves

To illustrate the approach, we assume that the overall kinesin biochemical cycle can be approximated by



(equation 3), where k_a and k_b are (lumped) rate constants. (A more general formalism can be found in the Theory section of Experimental Procedures). At low mechanical loads, each biochemical cycle is assumed to produce a single step of size $d = 8$ nm. The kinesin velocity at low loads will therefore be given by

$$v(c) = \frac{d}{(k_b)^{-1} + (k_a c)^{-1}}$$

(equation 4), where c is the concentration of ATP. Correspondence between equation 4 and the Michaelis–Menten expression (equation 2) is established through $v_{max} = d \cdot k_b$ and $K_m = k_b/k_a$. In an experiment, the relative magnitudes of the terms in the denominator of equation 4 may be changed by altering the ATP concentration.

For the case of tight coupling, we require that one (or both) of these terms increase with increasing external load, L . For example, if $k_b(L)$ happened to be the load-dependent rate, then the functional dependence of this term could be determined experimentally by measuring the force–velocity curve at saturating ATP, where $k_a c \gg k_b$. In this limit, the denominator term corresponding to k_a becomes negligible, and equation 4 reduces to $v(c) = d \cdot k_b(L)$. Knowledge of $k_b(L)$ could then be used to predict the shape of the force–velocity curve at limiting ATP, where $k_a c \ll k_b$. In general, this curve will display a very different shape from the corresponding curve at saturating ATP, independent of the particular load dependence of $k_b(L)$; the shapes of the force–velocity curves at saturating and limiting ATP are distinct. For example, for loads that are sufficient to reduce the velocity to half maximal at saturating ATP, the velocity at limiting ATP will have decreased by a factor approximately equal to $(1 - k_a c/k_b(0)) \approx 1$, i.e., hardly at all. Similarly, if $k_a(L)$ happened to be the load-dependent rate instead, then the functional dependence of this term could be determined by measuring the force–velocity curve at a limiting ATP concentration, such that $k_a c \ll k_b$, hence $v(c) = d \cdot k_a(L) \cdot c$. By a similar argument to the one just presented, the shapes of the force–

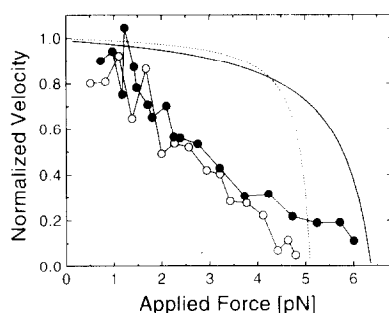


Figure 10. Normalized Force–Velocity Curves and Predictions Based upon Rate-Dependent Biochemistry (Tight Coupling Scenario)

Data from interferometry were normalized to the zero load velocity as determined from linear fits. The normalized force–velocity curve at saturating ATP concentrations (2 mM) (solid circles). The normalized force–velocity curve at limiting ATP concentrations (10 μ M) (open circles). First, for the case given by equation 8, an estimate of $X(L)$ was derived from a line fit of the normalized 2 mM ATP data (since $\tau_d \ll \tau_o$ at this ATP concentration, τ_d was neglected in the denominator of equation 6). Together with equation 8, this was used to predict the normalized force–velocity relationship at 10 μ M ATP (using $\tau_d/\tau_o = 9$ at 10 μ M ATP), shown by the solid line. Second, for the case given by equation 7, an estimate of $X(L)$ was derived from a line fit of the normalized 10 μ M ATP data (since $\tau_d \gg \tau_o$ at this ATP concentration, we neglect τ_o in the denominator of equation 5). Together with equation 5, this was used to predict the normalized force–velocity relationship at 2 mM ATP (using $\tau_d/\tau_o = 1/22$ at 2 mM ATP), shown by the dashed line.

velocity curves at saturating and limiting ATP concentrations will be quite distinct.

However, if both rate constants k_a and k_b were independent of load, then it follows that the net distance moved per ATP hydrolyzed would decrease according to

$$v = \frac{d}{((k_b)^{-1} + (k_a c)^{-1}) X(L)} \frac{1}{X(L)}$$

(equation 5), where $X(L)$ is some load-dependent factor, such that $X(L) \geq 1$, $X(0) = 1$, and $d \cdot X(L)^{-1}$ is the average distance moved per ATP. Equation 5 predicts that force–velocity curves, when normalized to the velocity at low loads, should all have the same shape. (Note: equation 5 also follows when both rate constants happen to have an identical dependence upon load, which can then be factored out; this possibility is addressed later.) Plotting our data in this fashion (Figure 10) shows that the load-independent model describes the data fairly well. Since the unitary step size of 8 nm is constant and fixed by the microtubule lattice, it seems appropriate to interpret the coupling ratio in equation 5, $\varepsilon = 1/X(L)$, as the probability that hydrolysis leads to a stepwise displacement. This, in turn, admits to at least two molecular-level interpretations: first, that kinesin molecules manage to make an 8 nm step only once every $1/\varepsilon$ cycles, or second, that each ATP hydrolysis produces one step, but there is a probability $(1-1/\varepsilon)$ per step that the molecule slips backward by exactly one step, i.e., that the motor works intermittently but cannot sustain load. Our data are not able to distinguish

clearly between these two possibilities. In some traces, slippage was clearly observed, but not in others (see Figures 7 and 8).

Under more general biochemical schemes than equation 3, the various different rate constants may be arranged into a mathematical form analogous to equation 4, with one set of constants dependent upon the ATP concentration and the other set independent of it. Although each of the terms in the denominator will be a complicated function of several biochemical rate constants, one can nevertheless apply similar reasoning to that just presented to exclude most tightly coupled models.

J. Howard and colleagues (personal communication) have recently measured single kinesin force–velocity curves using viscous agents to apply loads. In contrast with elastic forces, purely viscous loads cannot induce backward slippage, because viscous forces go to zero after a step is completed and the motor is at rest. Since their force–velocity curves resemble ours, we suspect that kinesin hydrolyzes ATP in a futile manner at high load. However, it is noteworthy that even for viscous loading, the kinesin molecule actually experiences an elastic load that decays with a damping time $\tau = \beta/\alpha$, where β is the drag coefficient of the load and α is a spring constant characterizing the linkage. Since this time could be as long as tens of milliseconds, much longer than the time required for the motor to make a step, the distinction between elastic and viscous loads becomes blurred. In vivo, it is unlikely that kinesin and related motors experience a significant viscous load (Luby-Phelps, 1993). During vesicular transport, the dominant load is almost certainly due to steric hindrance from elastic protein gels and membrane structures. During mitotic and meiotic movements (Hoyt, 1994), loads may also arise from elastic forces in strained MTs.

Our results are in broad agreement with the model of Leibler and Huse, which predicts a linear force–velocity curve for the case of strain-independent rate constants for transitions between states (Leibler and Huse, 1993). The shape of the force–velocity curve in that model follows from the fact that the step size decreases linearly with load, which is accommodated by placing a continuum of binding sites on the substrate. Such a continuum is an excellent approximation in the limit of large numbers of motors, but the model must be reformulated for single motors moving over discrete binding sites. Here, ATP hydrolysis induces a change in strain that will position a crossbridge between two binding sites in a way that is determined by load. The motor can subsequently rebind to the site from which it originated (more probable at high load), or attach to a distal binding site (more probable at low load). This model is therefore loosely coupled in the sense defined previously. The probability functions governing transitions will determine the shape of the force–velocity curve. Irrespective of such details, however, the strain independence of the rate constants in the Leibler–Huse model implies that normalized force–velocity curves are independent of ATP concentration, consistent with our data.

Comparison with Other Force Measurements

Earlier measurements using differing approaches provide divergent estimates of kinesin force. One experiment, using optical tweezers acting on a latex bead bound to a gliding MT whose motion was powered by a single kinesin molecule on a glass surface, gave an isometric force of 1.9 ± 0.4 pN (SD, $n = 14$) (Kuo and Sheetz, 1993). To slow the motor down, GTP, rather than ATP, was used to power motion. Short run lengths at high loads were found, as well as a load-dependent diminution in speed, both in qualitative agreement with our data. The quantitative discrepancy might be explained by several factors. First, the kinesin preparation may have had different properties, a possibility suggested by our observation of significant prep-to-prep variations (see Results). Second, GTP might not generate the same force as ATP, although in three instances, beads driven by ATP also produced ~ 2 pN. Third, calibration errors in determining optical forces may have been significant. Large distance from the coverglass affects trapping force, mainly owing to the increasing spherical aberration in light (Svoboda and Block, 1994), and it is unclear whether calibration experiments were carried out at the same distance from the coverglass surface as the actual assays, or adjusted for any possible differences. Fourth, the geometry of their assays was different, and the peak force produced by a kinesin motor along a MT might depend on the direction in which it is pulled (Figure 5; discussed in Results). Another experiment, using a sperm gliding assay and a centrifugal microscope, yielded a stall force of only 0.12 ± 0.03 pN (Hall et al., 1993). A force of this size would not permit single kinesin molecules to move longer MTs in vitro against their own viscous load ($F = 0.2$ pN for a microtubule 50 μm long moving at 500 nm/s [Brennen and Winet, 1977]). Kinesin from sea urchin rather than squid optic lobe was used in this study, and it is conceivable that this enzyme may be orders of magnitude weaker. It has also been suggested that the slowing of sperm heads moving in the centrifugal microscope may be due to something besides an inertial effect, and that the force thereby obtained is artifactually low (Hunt and Howard, 1993).

Recently, stepwise displacements and corresponding forces for the actomyosin system were reported, using both optical trapping (Finer et al., 1994) and flexible glass microneedle technologies (Ishijima et al., 1994). In the optical trapping work, single myosin displacements at relatively low mechanical loads followed a broad distribution, from <5 nm (the measurement noise limit) to ~ 17 nm, with an average value of 11 ± 2.4 nm (mean \pm SD). A similarly broad distribution of displacements was found using microneedles, with an extrapolated maximum displacement at zero force of ~ 17 nm. Single forces were also broadly distributed, ranging over roughly 1–8 pN in both experiments. The maximum force was estimated at ~ 5.7 pN using microneedles, and the average peak force was estimated at 3.4 ± 1.2 pN (mean \pm SD) using optical traps. Given the differing experimental approaches and conditions, these numbers are remarkably consistent. Indeed, they are not so very different from the displacements

(8 nm) and peak forces (5–6 pN) produced by kinesin motors. A force of ~ 5 pN, if maintained throughout the duration of an 8 nm step, dissipates some 40 pN \cdot nm of energy, which is roughly half of the available free energy of hydrolysis in a molecule of ATP (~ 80 pN \cdot nm). In a tightly coupled scenario, this dissipation would correspond to an overall thermodynamic efficiency of $\sim 50\%$ for a molecular motor.

Interestingly, Finer and colleagues found that the durations of single displacements (stepping times under low loads) were somewhat shorter than the durations of single forces under isometric conditions (tension times at high loads) at saturating ATP levels (cf. their Table 1). These data can be understood in terms of a model in which a kinetically significant rate constant decreases with strain. This is a molecular manifestation of the Fenn effect, whereby the energy released by muscle during active shortening is higher than during isometric contraction (Fenn, 1924; Bagshaw, 1993). In contrast with myosin, our data and modeling suggest that kinesin displays little if any Fenn effect; that is, the biochemical rates are relatively insensitive to applied load, and ATP hydrolysis continues at elevated rates even when motors are close to stall.

Experimental Procedures

Kinesin and Tubulin Preparation

Unless specified, reagents were from Sigma. Kinesin was purified from squid optic lobe by MT affinity as described (Vale et al., 1985), except that sucrose gradients (5%–25%) were run using a TLS-55 rotor and TL-100 tabletop ultracentrifuge (Beckman) for 4 hr at 55,000 rpm and 4°C (Bloom et al., 1988). Gradients were 2 ml, ~ 10 times larger than sample volumes. The ATP release step included 100 mM KCl. Kinesin was stored at -20°C in 50% glycerol with 2.5 mg/ml casein, 2.5 mg/ml cytochrome C, and 1 μM ATP. Stored in this fashion, kinesin was essentially unchanged for periods of up to 1 year. Tubulin was purified from bovine brain by MT affinity and phosphocellulose purified (Mitchison and Kirschner, 1984).

Bead Assays

Experiments were done at room temperature (22–23.5°C). Assay buffer (AB) contained 80 mM PIPES, 4 mM MgCl_2 , 1 mM EGTA, 50 mM KCl, 1 mM dithiothreitol, 1 mg/ml filtered casein, and 20 μM taxol (pH 6.9). Silica beads (5×10^7 per ml final concentration) were incubated in AB plus ATP (2 \times final concentration), 1 $\mu\text{g}/\text{ml}$ phosphocreatine kinase, and 2 mM phosphocreatine (>5 min) on a rotator at 4°C. In some experiments, the last three reagents were replaced by 1 mM AMP-PNP. The bead solution was rapidly mixed with an equal volume of kinesin (2 \times final concentration) in AB, followed by incubation on a rotator (~ 1 hr, 4°C). Final kinesin concentrations were typically 1:5,000 to 1:100,000 from stock (~ 50 $\mu\text{g}/\text{ml}$ kinesin heavy chain). Taxol-stabilized MTs were introduced into a flow chamber in which the lower coverslip had been treated with the silanizing reagent 4-ABDMS (Huls America). MTs bound tightly to this surface, mainly with their long axes parallel to the flow direction, thereby parallel to the direction of interferometer sensitivity (see text). The chamber was incubated with 1 mg/ml casein (in 80 mM PIPES, 4 mM MgCl_2 , 1 mM EGTA [pH 6.9]) for 5 min and subsequently washed with >5 vol of AB. Kinesin-coated beads were introduced at this stage.

Instrumentation

We used a modified inverted microscope (Axiovert 35, Carl Zeiss) equipped with Nomarski DIC optics (Plan Neofluar 100 \times /1.3NA oil objective) fixed to a vibration isolation table (Technical Manufacturing Corporation). Polarized light from a diode-pumped Nd:YLF laser (CW, 3W TEM₀₀, $\lambda = 1.047$ nm; TFR, Spectra Physics) was coupled into a polarization-preserving, single mode optical fiber (Oz Optics); this reduced laser pointing fluctuations. The fiber output coupler provided

a clean, collimated Gaussian beam of 5 mm diameter. Power levels were controlled by rotating a $\lambda/2$ plate followed by a fixed Gian-Laser polarizer. Beam steering was accomplished by small translations of the rear lens of a telescope arrangement (Svoboda and Block, 1994). To avoid fluctuations due to air currents or dust, the laser beam path was enclosed. An x - y piezo stage (P-775.00, Physik Instrumente) was used to position specimens with picometer precision under computer control. Experiments were controlled by a Macintosh computer equipped with a multifunction board (NB-M10-16H-9, National Instruments) running Labview software (National Instruments). The interferometer output was anti-alias filtered and digitized at 1 kHz, then stored on magneto-optical disks (DGR Technology). Data analysis was performed off line.

Displacement Measurement

Interferometer response was calibrated using an x - y piezo stage mounted with its y direction parallel to the interferometer shear axis. The piezo stage was driven by a computer-generated voltage sequence that produced a linear, triangle wave displacement (sawtooth) of the stage at a constant, slow speed (1.080 μm peak-peak; $v_s = 91 \pm 0.02 \mu\text{m/s}$; mean \pm SD, $n = 30$; nonlinearity $< \pm 3\%$). The required nonlinear voltage sequence for this movement was determined separately by nanometer-level video tracking of single beads bound to a coverglass and calibrated against a diamond-ruled grid with 10 μm spacing (Gelles et al., 1988; Svoboda et al., 1993). When a bead moves from the center of the detector toward its edge, the difference-over-sum signal, V_{out} , increases monotonically up to a saturation voltage, V_{max} , then begins to decrease (Denk and Webb, 1990). V_{max} occurred 280 nm from the center of the trap, but even for smaller displacements, the response curve (Figure 2a) displayed substantial nonlinearity. To determine distance up to ~ 200 nm from the center of the trap, the response curve was fit to the cubic equation $V_{\text{out}} = ay + by^2 + cy^3$. Corrected displacement, $y(t)$, was derived from $V_{\text{out}}(t)$ using a root of the fitted cubic. We define $q = a/3c - (b/3c)^2$ and $r = (ab) + V_{\text{out}}(t)c/6c^2 - (b/3c)^3$. Let $s_1 = (r + (q^2 + r^2)^{1/2})^{1/2}$ and $s_2 = (r - (q^2 + r^2)^{1/2})^{1/2}$. The displacement is $y(t) = -(s_1 + s_2)/2 - b/3c - i\sqrt{3}(s_1 - s_2)/2$. This procedure effectively linearized the response curve out to displacements of 200 nm and somewhat beyond (Figure 2b). In principle, a different response curve, parameterized by a particular set of the coefficients a , b , and c , is required for every particle size and focal position. Decreases in particle size or slight defocusing rescale the response by a factor < 1 . By measuring V_{max} , a unique set of coefficients can be found. Calibration experiments showed that a and c were linear functions of V_{max} , whereas b was independent of V_{max} : $a = 1.8 \times 10^{-3} \text{ V/nm} + (4.9 \times 10^{-3}/\text{nm})V_{\text{max}}$; $c = -3.37 \times 10^{-8} \text{ V}^2/\text{nm} - (42.38 \times 10^{-8} \text{ V/nm})V_{\text{max}}$; $b = 1.60 \times 10^{-5} \text{ V/nm}^2$. At high loads, V_{max} could not be measured, because beads never reached the edge of the trap. In this case, an averaged set of coefficients was used. To reduce errors arising from variations in bead size, we employed custom-made silica beads with low polydispersity ($0.520 \pm 0.007 \mu\text{m}$; mean \pm SD, $n = 20$; gifts of Egon Matijevic). Furthermore, the center of the trapping zone was adjusted to be ~ 250 nm above the focal plane of the microscope, so that by focusing on the MT, the optical trap was vertically centered on the bead. Control experiments with beads bound by AMP-PNP showed that this could be done with a high level of reproducibility. In other control experiments, beads stuck directly to the coverglass were moved through the detector zone at v_s ; displacement measurement errors were estimated to be $< \pm 5\%$ over the range 0–200 nm.

To characterize the elasticity of the kinesin-bead linkage, we used beads bound to MTs via kinesin in the presence of AMP-PNP. Results were identical to those obtained with beads attached in a rigorlike state in the absence of nucleotide. The stage was moved at v_s and the velocity of the bead, v_b , measured as a function of bead displacement. For each power level, the ratio $\langle v_b/v_s \rangle$ was derived from >250 velocity estimates using 10–15 beads.

At very low loads, kinesin velocity was measured using high resolution video tracking of the centroid of the bead (Gelles et al., 1988). Optical tweezers were used to place beads against microtubules, and the laser trapping light was shuttered as soon as movement began.

Laser Power at the Specimen Plane

To estimate the power delivered to the sample, we used $P = P_o \cdot T_o \cdot T_a$, where P_o is the power measured at a point before it enters the micro-

scope, $T_o = 0.58$ is the measured transmissivity of the microscope objective at 1.064 μm (Svoboda and Block, 1994), and $T_a = 0.86$ is the transmissivity of the back aperture of the objective for this optical setup, where the beam radius equals the aperture radius.

Force Measurement

To characterize the position-dependent optical load, we held a bead in the trap, typically 2 μm above the coverglass surface, and moved the chamber plus fluid in a sinusoidal motion at a large amplitude ($A = 1 \mu\text{m}$; calibrated by video tracking). For low frequencies, the applied force is $F = 2\pi\beta Af$, where f is the driving frequency. To compute β , we computed the viscosity of water from $\mu(T) = 1.456 \text{ cp} - 0.023 \text{ cp} \cdot T/^\circ\text{C}$ (Weast, 1987). Bead displacement with respect to the center of the trap was $y(t)$. Applied force as a function of the absolute value of $y(t)$ was linear out to 200 nm for 0.52 μm beads (Figure 2c); hence, α_r was constant. Determined in this way, $\alpha_r/P = 5.04 \pm 0.14 \times 10^{-4} \text{ pN/nm/mW}$ ($n = 20$, in water). A Brownian particle in a parabolic potential exhibits thermal fluctuations with a Lorentzian power spectrum, $S(f) = (kT/2\pi^2\beta)(f_0^2 + f^2)^{-1}$ where $\langle y^2(t) \rangle = 2\pi \int_0^\infty S(f) df$. Measurements of f_0 gave $\alpha_r/P = 5.28 \pm 0.14 \times 10^{-4} \text{ pN/nm/mW}$ ($n = 20$, in water), in close agreement with the former value. Insofar as possible, stiffness for every bead used was measured by the latter method during experiments. To monitor the change in stiffness with distance from the coverglass surface, we measured the mean square fluctuation in position and made use of the Equipartition Theorem, $\alpha_r = k_B T / \langle y^2(t) \rangle$, where $y(t)$ is the thermal displacement of the bead and $k_B T$ is the thermal energy. This estimate of α_r is independent of the drag, which changes dramatically at distances $h \leq a$, where h is the distance between the bead center and the surface: α_r was not found to change as we moved the trap close to the surface over the range 0–2 μm .

Two uncertainties in force measurements remain. First, in the motility assays, the bead is largely confined to the specimen plane, while during force calibration, unconstrained beads tend to move in the axial direction (down beam) toward the edge of the trap. For the beads used in these experiments, this movement was small, as judged by DIC microscopy, which has a depth of field of ~ 300 nm. Calculations suggest that the difference in maximal transverse force between the equilibrium plane and the specimen plane, i.e., the calibration error, is also small ($< 5\%$) (Ashkin, 1992). Second, the optical force applied to the bead tends to torque the bead about its point of attachment to the MT, increasing the bead interaction with the glass and MT surfaces (Figure 3). Since beads rarely stuck to the surface, this interaction may be considered a surface-enhanced drag. Tension in the tether tends to pull the bead toward the surface. For the largest trap stiffnesses used in these experiments, the mean square distance from the surface due to thermal agitation is $\sqrt{\langle z^2 \rangle} > 10$ nm. This implies a drag enhancement of $\xi = 2$ –3, corresponding to a total viscous force < 0.01 pN at kinesin velocities of ~ 600 nm/s. The surface-enhanced drag is therefore negligible.

Optical forces in assay buffer were slightly smaller than in water (Figure 2d), $\alpha_r/P = 4.90 \pm 0.10 \text{ pN/nm/mW}$ ($n = 50$; determined from Brownian fluctuations), an effect stemming from the increase in the index of refraction due to dissolved salt and protein. Whenever a bead became stuck or was lost before trapping stiffness could be determined, we used this stiffness to compute forces.

Construction of Force-Velocity Curves

Interferometer output was converted to distance as described above. Bead displacements over the range 50–200 nm were used for analysis. Bead velocities were computed and corrected for the linkage compliance (Figure 5). To compute velocity, individual displacement records were averaged over either 50 ms or 20 ms intervals, at 10 μM ATP or 2 mM ATP, respectively, reducing Brownian noise. Line fits were made to successive 20 nm segments of these records, and the velocity for each such segment was determined as well as the mean force during the segment. Velocities were then binned at fixed intervals of force and plotted against average force. The high load force-velocity curve was constructed from 50 runs at 15 mW, 45 runs at 30 mW, and 169 runs at 62.5 mW. The low load force-velocity curve was constructed from 9 runs at 15 mW, 13 runs at 30 mW, and 17 runs at 62.5 mW.

Phenomenological Theory

The ATP-dependent kinesin velocity at low loads has been shown to obey a Michaelis-Menten-type relation, which can be recast as

$$v_d(c) = \frac{\epsilon_0 d}{\tau_0 + \tau_d(c)}$$

(equation 6), where ϵ_0 is the coupling ratio at low loads, defined earlier. τ_0 is independent of c , while $\tau_d(c) = \phi/c$, and both quantities have units of time: in general, ϕ and τ_0 are complicated functions of the biochemical rate constants (Johnson, 1992). Correspondence between equation 3 and the Michaelis-Menten expression (equation 2) is established through $v_{max} = \epsilon_0 d/\tau_0$ and $K_m = \phi/\tau_0$. Since clustering of 8 nm steps is not observed at limiting ATP concentrations (Svoboda et al., 1993), we assume $\epsilon_0 < 1$. For example, if two ATP molecules are hydrolyzed for every 8 nm step, then $\epsilon_0 = 1/2$.

How does an external load enter into equation 6? The unitary step size is presumably fixed by the MT lattice and is thereby independent of load. Since increasing load decreases the velocity, some load-dependent factor ($X(L)$, defined earlier) must multiply one (or both) of the times in the denominator of equation 6. Consider first the case where the ATP turnover rate is reduced in direct proportion to the motor velocity as load increases. This corresponds to a tightly coupled situation, and the overall motor efficiency increases with load until it is maximal approaching stall. The implications of this assumption for the shapes of the force-velocity curves in the context of a simplified kinetic scheme (equation 1) are discussed in the text. In the general case, however, our analysis depends only on being able to group the biochemical rates into two lumped functions (τ_0 and τ_d in equation 6), one of which is independent of the ATP concentration, and the other of which is inversely proportional to it. In addition, τ_0 and τ_d have to be functions of distinct subsets of the kinetic rate constants. The ability to perform this decomposition into τ_0 and τ_d depends upon three additional facts: first, hydrolysis reversals do not occur ($k_{-2} = 0$) (Hackney, 1988); second, ADP release is irreversible ($k_{-4} = 0$), a reasonable assumption for the very low ADP concentrations present in our assays; and third, ADP release is at least partially rate limiting ($k_4 < k_2, k_3$) (Hackney, 1988). For the simplified kinetic scheme of equation 1, $\tau_0 = k_2^{-1} + k_3^{-1} + k_4^{-1}$ and $\tau_d = (k_{-1} + k_{-2})/k_1 k_2 c$. The mean time between ATP hydrolysis and ADP release is $(\tau_0 - 1/k_2)$, while the mean time between ADP release and ATP hydrolysis is $(\tau_d + 1/k_2)$. The time scale containing the load-dependent rate constant will depend on load and hence can be written in the form $\tau(L) = \tau \cdot X(L)$, where $X(L)$ can be measured. For example, if k_{-1} increases with load, or if k_2 or k_3 decrease with load, then

$$v(c, L) = \frac{\epsilon_0 d}{\tau_0 + \tau_d(c) X(L)}$$

(equation 7). At limiting ATP, where $\tau_d \gg \tau_0$, the factor $X^{-1}(L)$ is simply the force-velocity curve normalized to unity at zero load (Figure 9b).

Given a measurement of the force-velocity curve at limiting ATP and a knowledge of K_m , we can then predict the shape of the force-velocity curve for saturating ATP, where $\tau_d \ll \tau_0$. For our data at 2 mM ATP, we estimate $\tau_d \approx \tau_0/22$. At this concentration, velocity will not decrease appreciably until loads become such that $X(L) \approx 20$. Under limiting ATP conditions, the velocity will have decreased roughly 20-fold for similar loads. Therefore, the force-velocity curves will have distinctively different shapes at the two different ATP concentrations, as illustrated in Figure 10.

If either k_2, k_3 , or k_4 decreases with increasing load, then

$$v(c, L) = \frac{\epsilon_0 d}{\tau_0 X(L) + \tau_d(c)}$$

(equation 8). In this case, the factor $X^{-1}(L)$ is now identified as the force-velocity curve normalized to unity at saturating ATP. Similar arguments to those just made above show that the predicted force-velocity curves at limiting ATP will have a distinctly different shape from that at saturating ATP (Figure 10).

There are two possible mechanisms that accommodate load-dependent biochemistry and nevertheless lead to equation 4 (see text),

thereby accounting for the experimental data. First, the rate constants in equation 1 might depend upon load in such a way that τ_d and τ_0 are both modified with load by the same multiplicative factor, allowing $X(L)$ to be factored out in the denominator and reproducing equation 4. For example, if strain modified the rate for ADP release and ATP binding in an identical manner, i.e., if $k_1(L) \propto k_4(L)$ and $k_4 \ll k_2, k_3$, it is conceivable that such a scenario would hold. Note that this scheme requires that ATP binding energies increase with load, while ADP binding energies decrease in similar proportion. We consider this scenario to be an unlikely explanation for the data. Second, strain might act upon k_2 alone, with $k_1 \gg k_2$ and $k_2 \gg k_3, k_4$. In this case, both time scales (τ_d and τ_0) in the denominator of equation 6 would be multiplied by $X(L)$, again leading to equation 4. However, kinetic studies have shown that ADP release is at least partially rate limiting (Hackney, 1988), implying $k_2 < k_4$, invalidating this explanation. If the kinesin mechanochemistry were largely load independent, on the other hand, then a diminution in velocity with load implies that a decreasing fraction of hydrolysis cycles leads to stepping. In this case, the mean time per step is $(\tau_d + \tau_0)X(L)$, which leads naturally to equation 4.

Acknowledgments

We thank Howard Berg, Richard Berry, David Huse, Stan Leibler, George Oster, and Aravi Samuel for helpful discussions, Christoph Schmidt, Bruce Schnapp, and Russell Stewart for help with motility assays, and Egon Matijevic for the gift of silica beads. This work was supported by the Rowland Institute for Science.

Received March 18, 1994; revised April 20, 1994.

References

- Ashkin, A. (1992). Forces of a single-beam gradient laser trap on a dielectric sphere in the ray optics regime. *Biophys. J.* 61, 569-582.
- Ashkin, A., Dziedzic, J. M., Bjorkholm, J. E., and Chu, S. (1986). Observation of a single-beam gradient force optical trap for dielectric particles. *Opt. Lett.* 11, 288-290.
- Bagshaw, C. R. (1993). *Muscle Contraction* (New York: Chapman and Hall).
- Bevington, P. R. (1969). *Data Reduction and Error Analysis for the Physical Sciences* (New York: McGraw-Hill).
- Block, S. M., Goldstein, L. S. B., and Schnapp, B. J. (1990). Bead movement by single kinesin molecules studied with optical tweezers. *Nature* 348, 348-352.
- Bloom, G. S., Wagner, M. C., Pfister, K. K., and Brady, S. T. (1988). Native structure and physical properties of bovine brain kinesin and identification of the ATP-binding subunit polypeptide. *Biochemistry* 27, 3409-3416.
- Brennen, C., and Winet, H. (1977). Fluid mechanics of propulsion by cilia and flagella. *Annu. Rev. Fluid Mech.* 9, 339-398.
- Burton, K. (1992). Myosin step size: estimates from motility assays and shortening muscle. *J. Muscle Res. Cell Motil.* 13, 590-607.
- Cohn, S. A., Ingold, A. L., and Scholey, J. M. (1987). Correlation between the ATPase and microtubule translocating activities of sea urchin egg kinesin. *Nature* 328, 160-163.
- Denk, W., and Webb, W. W. (1990). Optical measurements of picometer displacements of transparent microscopic objects. *Appl. Opt.* 29, 2382-2390.
- Fenn, W. O. (1924). The relation between the work performed and the energy liberated in muscular contraction. *J. Physiol. (London)* 184, 373-395.
- Finer, J. T., Simmons, R. M., and Spudis, J. A. (1994). Single myosin molecule mechanics: piconewton forces and nanometre steps. *Nature* 368, 113-119.
- Gelles, J., Schnapp, B. J., and Sheetz, M. P. (1988). Tracking kinesin-driven movements with nanometre-scale precision. *Nature* 331, 450-453.
- Gilbert, S. P., and Johnson, K. A. (1993). Expression, purification, and characterization of the *Drosophila* kinesin motor domain produced in *Escherichia coli*. *Biochemistry* 32, 4677-4684.

- Hackney, D. D. (1988). Kinesin ATPase: rate-limiting ADP release. *Proc. Natl. Acad. Sci. USA* **85**, 6314–6318.
- Hackney, D. D. (1994). Alternating head catalysis by kinesin during microtubule-stimulated ATP hydrolysis. *Biophys. J.* **66**, 311a.
- Hackney, D. D., Malik, A. S., and Wright, K. W. (1989). Nucleotide-free kinesin hydrolyzes ATP with burst kinetics. *J. Biol. Chem.* **264**, 15943–15948.
- Hackney, D. D., Levitt, J. D., and Wagner, D. D. (1991). Characterization of a2b2 and a2 forms of kinesin. *Biochem. Biophys. Res. Commun.* **174**, 810–815.
- Hackney, D. D., Levitt, J. D., and Suhan, J. (1992). Kinesin undergoes a 9S to 6S conformational transition. *J. Biol. Chem.* **267**, 8696–8701.
- Hall, K., Cole, D. G., Yeh, Y., Scholey, J. M., and Baskin, R. J. (1993). Force–velocity relationships in kinesin-driven motility. *Nature* **364**, 457–459.
- Hirokawa, N., Pfister, K. K., Yurifuji, H., Wagner, M. C., Brady, S. T., and Bloom, G. S. (1989). Submolecular domains of bovine brain kinesin identified by electron microscopy and monoclonal antibody decoration. *Cell* **56**, 867–878.
- Howard, J., Hudspeth, A. J., and Vale, R. D. (1989). Movement of microtubules by single kinesin molecules. *Nature* **342**, 154–158.
- Hoyt, M. A. (1994). Cellular roles of kinesin and related proteins. *Curr. Opin. Cell Biol.* **6**, 63–68.
- Hunt, A. J., and Howard, J. (1993). Kinesin swivels to permit microtubule movement in any direction. *Proc. Natl. Acad. Sci. USA* **90**, 11653–11657.
- Huxley, A. F. (1957). Muscle structure and theories of contraction. *Prog. Biophys. Biophys. Chem.* **7**, 255–318.
- Ishijima, A., Harada, Y., Kojima, H., Funatsu, T., Higuchi, H., and Yanagida, T. (1994). Single-molecule analysis of the actomyosin motor using nano-manipulation. *Biochem. Biophys. Res. Commun.* **199**, 1057–1063.
- Johnson, K. A. (1992). Transient-state kinetic analysis of enzyme reaction pathways. In *The Enzymes*. (New York: Academic Press), pp. 1–61.
- Kamimura, S., and Mandelkow, E. (1992). Tubulin protofilaments and kinesin-dependent motility. *J. Cell Biol.* **118**, 865–875.
- Kuo, S. C., and Sheetz, M. P. (1993). Force of single kinesin molecules measured with optical tweezers. *Science* **260**, 232–234.
- Kuznetsov, S. A., and Gelfand, V. I. (1986). Bovine brain kinesin is a microtubule-activated ATPase. *Proc. Natl. Acad. Sci. USA* **83**, 8530–8534.
- Leibler, S., and Huse, D. A. (1993). Porter versus rowers: a unified stochastic model of motor proteins. *J. Cell Biol.* **121**, 1357–1368.
- Luby-Phelps, K. (1993). Physical properties of cytoplasm. *Curr. Opin. Cell Biol.* **6**, 3–9.
- Mitchison, T., and Kirschner, M. (1984). Microtubule assembly nucleated by isolated centrosomes. *Nature* **312**, 232–237.
- Oosawa, F., and Hayashi, S. (1986). The loose coupling mechanism in molecular machines of living cells. *Adv. Biophys.* **22**, 151–183.
- Ray, S., Meyhofer, E., Milligan, R. A., and Howard, J. (1993). Kinesin follows the microtubule's protofilament axis. *J. Cell Biol.* **121**, 1083–1093.
- Schnapp, B. J. (1986). Viewing single microtubules by video light microscopy. *Meth. Enzymol.* **134**, 561–573.
- Scholey, J. M., Heuser, J., Yang, J. T., and Goldstein, L. S. B. (1989). Identification of globular mechanochemical heads of kinesin. *Nature* **338**, 355–357.
- Svoboda, K., and Block, S. M. (1994). Biological applications of optical forces. *Annu. Rev. Biophys. Biomol. Struct.* **23**, 247–285.
- Svoboda, K., Schmidt, C. F., Schnapp, B. J., and Block, S. M. (1993). Direct observation of kinesin stepping by optical trapping interferometry. *Nature* **365**, 721–727.
- Taylor, E. W. (1993). Variations on the theme of movement. *Nature* **361**, 115–116.
- Vale, R. D., Reese, T. S., and Sheetz, M. P. (1985). Identification of a novel force-generating protein, kinesin, involved in microtubule-based motility. *Cell* **42**, 39–50.
- Weast, R. C., ed. (1987). *CRC Handbook of Chemistry and Physics, Sixty-Seventh Edition* (Boca Raton, Florida: CRC Press).
- Yanagida, T., Arata, T., and Oosawa, F. (1985). Sliding distance of actin filament induced by a myosin crossbridge during one ATP hydrolysis cycle. *Nature* **316**, 366–369.
- Yanagida, T., Harada, Y., and Ishijima, A. (1993). Nano-manipulation of actomyosin molecular motors in vitro: a new working principle. *Trends Biochem. Sci.* **18**, 319–324.